arXiv:1701.02407v1 [astro-ph.SR] 10 Jan 2017

Material supply and magnetic configuration of an active region filament

P. Zou[1,2,3], C. Fang[1,2,3], P. F. Chen[1,2,3], K. Yang[1,2,3], Q. Hao[1,2,3], & Wenda Cao[4]

fangc@nju.edu.cn

Received _____; accepted _____

[1]School of Astronomy & Space Science, Nanjing University, Nanjing 210023, China

[2]Key Lab of Modern Astronomy & Astrophysics (Nanjing University), Ministry of Education, Nanjing 210023, China

[3]Collaborative Innovation Center of Modern Astronomy and Space Exploration, Nanjing 210023, China

[4]Big Bear Solar Observatory, New Jersey Institute of Technology, 40386 North Shore Lane, Big Bear City, CA 92314, USA

ABSTRACT

It is important to study the fine structures of solar filaments with high-resolution observations since it can help us understand the magnetic and thermal structures of the filaments and their dynamics. In this paper, we study a newly-formed filament located inside the active region NOAA 11762, which was observed by the 1.6 m New Solar Telescope (NST) at Big Bear Solar Observatory (BBSO) from 16:40:19 UT to 17:07:58 UT on 2013 June 5. As revealed by the Hα filtergrams, cool material is seen to be injected into the filament spine with a speed of 5–10 km s^{-1}. At the source of the injection, brightenings are identified in the chromosphere, which is accompanied by magnetic cancellation in the photosphere, implying the importance of magnetic reconnection in replenishing the filament with plasmas from the lower atmosphere. Counter-streamings are detected near one endpoint of the filament, with the plane-of-the-sky speed being 7–9 km s^{-1} in the Hα red-wing filtergrams and 9–25 km s^{-1} in the blue-wing filtergrams. The observations are indicative of that this active region filament is supported by a sheared arcade without magnetic dips, and the counter-streamings are due to unidirectional flows with alternative directions, rather than due to the longitudinal oscillations of filament threads as in many other filaments.

Subject headings: Sun: chromosphere — Sun: filaments — Sun: magnetic configurations

1. INTRODUCTION

Solar filaments, called prominences when seen above the solar limb, look like cool and dense clouds suspended in the solar corona. They are always located near the polarity inversion lines (PILs), thus can be used to trace the large-scale pattern of weak background magnetic field (Low 1982; Minarovjech et al. 1998). The long-lived quiescent filaments can also be used to trace the solar differential rotation (Gigolashvili et al. 2013). Once they erupt, solar filaments are often associated with solar flares (e.g., Martin & Ramsry 1972; Schmahl 1982) and/or coronal mass ejections (CMEs, St. Cyr & Webb 1991; Chen 2011). Many authors have analyzed their formation, oscillation, eruption, their interaction with other activities, and the long-term statistical properties (Moore & Roumeliotis 1992; Manchester et al. 2008; Schmieder et al. 2013; Hao et al. 2015).

One important issue in the filament research is their formation mechanisms, which have been studied for decades (e.g., Smith & Priest 1977). Generally speaking, there are three possible mechanisms accounting for the filament formation (Mackay et al. 2010). The first and also the most popular one is the evaporation-condensation model. This model has been extensively studied by many authors using numerical simulations (Antiochos et al. 1999; Karpen et al. 2001, 2005, 2006; Karpen & Antiochos 2008; Xia et al. 2012, 2014; Zhou et al. 2014). The merit of this model is that it can naturally explain the sudden appearance of the dense cool plasma suspended in the tenuous hot corona (Berger et al. 2012; Liu et al. 2012). The second one is the levitation model, which was initially proposed by Rust & Kumar (1994). However, so far there are only a few observations which can fit into this model (Lites 2005; Okamoto et al. 2008; Yelles et al. 2012). For example, Lites & Low (1997) observed a filament being formed after the emergence of a δ-sunspot and suggested that the cool material is dragged up into the corona through the levitation process. Instead of being levitated as a whole, it was proposed that the chromospheric plasmas might be lifted

up through tornadoes, which are the feet of the filaments (Li et al. 2012; Su et al. 2012). The third one is the injection model, which suggests that cool material is ejected from the chromosphere into the corona via magnetic reconnection (Wang 1999). Some observations revealed strong flows moving into active-region filaments, which tend to support this model (Chae 2003; Schmieder et al. 2004). However, it seems that the larger and higher quiescent filaments are not formed by this mechanism (Karpen 2015). This is probably because that the injection speed of the cool plasma is not high enough for the materials to reach the magnetic dips of a quiescent filament. In this sense, the velocity measurements of the cool material around filaments are important for understanding the feasibility of the injection mechanism.

One interesting feature of the filament dynamics is the counter-streamings (Zirker et al. 1998). A natural interpretation is that the counter-streamings are caused by longitudinal oscillations of filament threads (Karpen et al. 2006; Xia et al. 2011). In this case, a magnetic dip is needed, which was originally proposed to support the apparently static filament in the low-resolution images. The magnetic dips may exist in a flux rope (Kuperus & Raadu 1974) or a sheared arcade (Kippenhahn & Schlüter 1957). However, with numerical simulations, Karpen et al. (2001) proposed that a magnetic dip is not necessary for supporting a filament, where cool plasmas repeatedly appear and disappear near magnetic PILs. In this case, longitudinal oscillations are not sustainable, so the counter-streamings, which were found to be universal in both quiescent and active region filaments, may be due to large-scale unidirectional flows, which have opposite moving directions in neighboring flux tubes, as proposed by Chen et al. (2014b). However, there is still lack of evidence that counter-streamings are in the form of unidirectional flows with alternative directions. Since a quiescent filament is typically supported by a magnetic flux rope where magnetic dips are always present, it is expected that the unidirectional flow-based counter-streamings can be seen only in active region filaments.

As the spatial resolution increases, observations are providing more and more detailed structures and dynamics of solar filaments, which are helpful to unveil the formation mechanism and the material circulation in filaments. In this paper, we use observations from the current largest solar telescope, 1.6 m New Solar Telescope (NST, Cao et al. 2010; Goode & Cao 2012), at the Big Bear Solar Observatory (BBSO) to analyze the material flows in a newly-formed filament by tracing its fibrils. It is expected to give an insight into the questions about where the filament material comes from and how the counter-streamings are formed in the filament. The observations are described in Section 2. The results are given in Section 3. The discussions and the summary are presented in Section 4.

2. OBSERVATIONS

The newly-formed filament was located in the active region NOAA 11762 (S28W62) on 2013 June 5. Its formation is well recorded by the Atmospheric Imaging Assembly (AIA, Lemen et al. 2012) in EUV and the Global Oscillation Network Group (*GONG*) in Hα (Harvey et al. 2011). AIA is on board the *Solar Dynamics Observatory* (*SDO*). The AIA telescope has a pixel size of $0\farcs6$ with a time cadence of 12 s. As indicated by the arrow in Figure 1(b), the filament is first seen in AIA 304 Å at 13:55 UT. At that time, nothing is visible in Hα, as shown by Figure 1(e). The filament spine becomes visible in Hα after 16:00 UT, as indicated by Figure 1(f).

The filament was also observed by the NST at BBSO from 16:40:19 UT to 17:07:58 UT with a much higher resolution. The field of view (FOV) is centered at (647″, -482″) in the heliocentric coordinates. NST consists of a suite of instruments. Its Broadband Filter Imager (BFI) uses a TiO filter (7057 Å) to obtain the white-light images with a bandpass of 10 Å. It has a time cadence of 15 s. The diffraction-limited resolution is $0\farcs11$ and the pixel size is $0\farcs034$. The filtergrams at Hα line center, H$\alpha\pm$0.2 Å, $\pm$0.6 Å, and $\pm$1.0 Å are

acquired by the Visible Image Spectrometer (VIS). The VIS uses a Fabry-Pérot etalon with the bandpass of 0.07 Å. Its FOV is $70'' \times 70''$. The diffraction limited resolution is $0''.1$ and the pixel size is $0''.03$.

To understand the magnetic environment of the filament formation and its flows, we use the magnetograms observed by the Helioseismic and Magnetic Imager (HMI, Scherrer et al. 2012; Schou et al. 2012) on board the *SDO*. In particular, one special product of the HMI data, i.e., the Space-weather HMI Active Region Patches (SHARPs, Bobra et al. 2014), is used, where the minimum energy method is adopted to resolve the 180° ambiguity (Metcalf 1994; Metcalf et al. 2006). The Lambert method is applied to modify the coordinate system (Bobra et al. 2014), and the projection effects are corrected with the method used by Gary & Hagyard (1990).

3. RESULTS

Using the AIA 4500 Å and NST TiO images, we co-align the images in TiO and Hα with the magnetograms observed by *SDO*/HMI. Figure 2 displays the co-aligned magnetogram (*left panel*), white-light image in TiO (*middle panel*), and the Hα center filtergram (*right panel*). The rough location of the filament is bracketed by two white lines. It can be seen that the filament is located near the magnetic PIL between two sunspots, with the southern endpoint near the sunspots and the other endpoint outside the field of view (FOV). The filament has an "S"-shaped structure, a typical one with positive helicity mainly in the southern hemisphere. As seen from the right panel of Figure 2, this filament has many right-bearing barbs, and the threads are right bearing as well.

3.1. Plasma motion and bright patches

In the Hα line-wing images, we can identify many moving fibrils on both sides of the filament spine. In Figure 3(a), we select three small regions, which are displayed in panels (b)–(d), respectively. Several moving fibrils can be clearly seen in the Hα line-wing filtergrams, as marked by the dashed lines in Figures 3(b)–(d). In all these fibrils, materials are seen to be injected toward the filament spine. One strange feature is that the fibrils on the two sides of the filament spine are far from being parallel. They even have opposite senses of bearing, according to the definition by Martin et al. (1994), i.e., the fibrils on the east side are right-bearing, whereas those on the west side are left-bearing.

After examining Figure 3 and the associated movie, we found that the material injections along the fibrils generally originate from bright regions. In order to illustrate it, we plot the Hα center filtergram in Figure 4(a), where the areas with intensity enhancement are highlighted with yellow contours as done in Figure 3(a). Inside the red rectangular box, the brightness is integrated over all the pixels with relative intensity higher than 2 (the averaged intensity of the background is set to be unity), and the temporal evolution of the integrated intensity is shown in panel (c) as the solid line. It is seen that the integrated brightness changes drastically with time. At the same time, the underlying photospheric magnetic field also changes. In order to check whether they are related to each other, we select the blue rectangular box in Figure 4(b) to calculate the total negative magnetic flux inside the box. The blue box is shifted from the red one after considering the projection effects and assuming that the Hα formation layer is about 2000 km above the photosphere where the magnetic field is measured. The variation of the negative magnetic flux inside the blue box is displayed in panel (c) as the dashed line. It can be seen in Figure 4(c) that almost each episode of Hα brightening is preceded by magnetic flux cancelation. Using the cross-correlation method, the lightcurve and the negative magnetic flux evolution are

found to be negatively correlated, with the maximum correlation coefficient being -0.76 when the time delay between the lightcurve and the magnetic flux is set to be 320 s. That is to say, each time when magnetic cancelation happens, Hα brightness increases about 320 s later. Thus, we conjecture that the brightening of the filament channel is possibly caused by magnetic field cancelation. It is noted that since the resolution of our Hα observations is about twenty times higher than that of the HMI magnetogram, it is nearly impossible to compare the detailed structure in Hα filtergrams with that in the magnetogram. To establish a more quantitative relation between the magnetic cancelation and the chromospheric heating, future magnetograms with higher resolutions are needed.

Now we select one typical fibril to analyze its dynamics. This fibril, labeled fibril 1, is located on the west side of the filament spine, as shown in Figure 3(b). A slice is placed along fibril 1 in Figure 5(a). The time-distance diagram of the Hα intensity along this slice is displayed in Figure 5(b). Since the flow is more evident in the Hα line wing and the chromospheric brightening is more visible in the Hα line center, H$\alpha + 0.6$ Å intensity image is used for the top half distance, whereas Hα center intensity image is used for the bottom half distance. It is seen that several moving fibrils exist in the top half distance and several Hα brightenings exist in the bottom half distance. It is indicative of that the ejection and the brightening should be physically connected. We tentatively draw three green arrows in order to match Hα fibrils with the corresponding brightenings. Besides, there are another two moving fibrils at $t = 10$ s and 150 s, which should be related to chromospheric heating before and after our observations, respectively.

It can be seen in Figure 5 that the material injections are episodic. Each fibril lasts for about 100–200 s. The injection velocities are measured to be about 5–10 km s^{-1}. Chae (2003) proposed that reconnection-driven jets in the low atmosphere might be able to supply mass for the formation of a solar filament. The fibrils revealed by our Figure 5 tend

to support such a scenario.

3.2. Counter-streamings and magnetic configuration

In contrast to the main spine where threads are highly sheared and overlapping with each other, the threads near the southern endpoint of the filament are more clearly separated, which offers a good chance to study their dynamics. The Hα movie indicates that these threads are filled with moving materials. In order to investigate their dynamics, we choose two slices and display their time-distance plots in different wavelengths in Figure 6. Both slices start from the spine (bottom right) to the endpoint (upper left) following the threads near the filament endpoint. It can be seen that along the red slice, repetitive cool plasma flows move to the south. On the contrary, the cool plasma in the yellow slice moves to the north. We further select several other slices covering different threads, and calculate the moving velocities based on time-distance diagrams. The resulting velocities are plotted as arrows superimposed on the Hα filtergram in Figure 7. The length of each arrow represents the amplitude of the velocity of the plasma flow, and the color indicates which off-line filtergram can best show the moving plasma. The velocity pattern in Figure 7 is strongly reminiscent of the counter-streamings discovered by Zirker et al. (1998). The velocities of the southward flows are about 7–9 km s^{-1} and those of the northward flows are about 9–25 km s^{-1} (see Figure 7).

4. DISCUSSIONS

4.1. Mass supply and counter-streamings

The formation mechanism of solar filaments is an important issue in filament research (Parenti 2014). Although an individual author might favor one mechanism, it seems that

filaments may be formed in different ways. For those filaments that condense in situ in the corona (Liu et al. 2012), the thermal nonequilibrium model works well (Karpen et al. 2006; Xia et al. 2011, 2012), which can qualitatively explain the in-situ brightening successively from high-temperature extreme ultraviolet (EUV) lines to low-temperature EUV lines, and all the way to the Hα line (Chen 2014a). According to this model, chromospheric plasma is evaporated into the corona due to localized heating, forming hot and dense coronal loops. When the density reaches a threshold, thermal instability is triggered, and the hot plasma cools drastically to form cool plasma suspended in the corona. On the other hand, there are also accumulative examples of filament formation via injection, i.e., cool chromospheric plasmas are injected into the corona as a result of magnetic reconnection (Chae 2003; Schmieder et al. 2004). In this case, the typical features include (1) low atmosphere brightening can be seen in Hα or even EUV; (2) cold plasma is driven from the chromosphere to the corona so as to supply materials for the filament. Our observations presented in this paper are consistent with this model.

We found that on the both sides of the filament channel, there are sustaining brightening visible in Hα line-center images. From time to time, materials are injected upward from these bright patches to replenish the filament spine with a velocity of about 5–10 km s^{-1}. In particular, near the south endpoint of the filament, the injected materials form the threads of the filament directly. The injections are intermittent, with an interval from tens of seconds to several minutes. Each injection lasts for about 100–200 s, preceded by an enhanced brightening in Hα at the source site, indicating localized heating in the chromosphere. Note that the ejected materials move upward along the magnetic field and should be observed as blue-shift if the ejection is toward the observer. However, the flows are observed to be red-shifted. The reason is that this active region is located in the southwest quadrant of the solar disk, and the magnetic field lines are bent away from the observer (as indicated by Figure 8b). As a result, the upward-moving materials are

observed to be red-shifted. Compared with the photospheric magnetograms, it is found that the brightening is almost always associated with magnetic cancelation, implying that magnetic reconnection is happening in the low atmosphere (Wang et al. 2009). A rough estimation indicates that the injection velocity is too small to lift the material into the corona if the plasma experiences a ballistic motion with the gravity acting on it only. The fact that the cool materials keep moving without significant deceleration implies that there must be additional forces acting on the flows. Since the cold plasma flows move along the magnetic field, the Lorentz force does not help. A possible source of the additional forces could be the higher gas pressure in the source region. Through 3D magnetohydrodynamics (MHD) numerical simulations, Jiang et al. (2011) found that whereas the reconnection jet is accelerated initially by magnetic tension force, its later evolution is dominated by the gas pressure gradient. In our observations, chromospheric brightenings appear in the source site of the injection. Its enhanced gas pressure might provide an additional force to sustain the moving materials against gravity. The enhanced pressure may even trigger a shock wave, which can effectively push the fibrils upward (Ryutova et al. 2008).

As the characteristic dynamics of a filament in the quiescent state, counter-streamings are generally explained in terms of longitudinal oscillations of filament threads (Lin 2003). It is generally believed that there exist dips in the magnetic field of the filaments, which enable the gravity to be a restoring force and facilitate the longitudinal oscillations (Luna & Karpen 2012; Zhang et al. 2012). However, inspired by the observations showing that filaments are always in a dynamic state, Karpen et al. (2001) pointed out that magnetic dips might not be a necessary condition for filaments. They proposed that, driven by asymmetric heating at the two footpoints of a magnetic tube, chromospheric plasma is evaporated into the corona. The condensed hot gas cools down to form a filament thread. After staying in the corona for some time, the filament thread is pushed by the gas pressure imbalance between the two footpoints of the magnetic tube, draining down toward the footpoint with

weaker heating. In this model, an ensemble of threads like this form the counter-streamings. The observations displayed by Liu et al. (2012) seem to support such a dynamic picture, i.e., filament materials are circulated via chromospheric evaporation, coronal condensation, and mass drainage. In this paper, we presented another scenario: cold chromospheric materials are intermittently injected into the corona from one footpoint of a magnetic tube, which run through the flux tube in the corona and then fall down toward the other footpoint. A random distribution of the injection sources results in alternative flows from the positive to the negative polarities and the other way around, leading to counter-streaming pattern displayed in Figure 7. In this scenario, no chromospheric evaporation is required.

4.2. Magnetic Configuration

Two types of magnetic configurations have been proposed for solar filaments, i.e., a flux rope (Kuperus & Raadu 1974) and a sheared arcade (Kippenhahn & Schlüter 1957). Traditionally, the difference between these two configurations can be distinguished by measuring the magnetic component of filament threads perpendicular to the magnetic PIL. That is, the flux rope corresponds to a magnetic field with inverse polarity, whereas the sheared arcade corresponds to a magnetic field with normal polarity. Recently, Chen et al. (2014b) proposed an indirect method to infer the magnetic configuration of a filament: a filament with left-bearing barbs and positive helicity (or with right-bearing barbs and negative helicity) is supported by a flux rope, whereas a filament with right-bearing barbs and positive helicity (or with left-bearing barbs and negative helicity) is supported by a sheared arcade[1]. With the method proposed by Chen et al. (2014b), Ouyang et al. (2015) and Hao et al. (2016) identified the magnetic configurations of several filaments, with some

[1]It should be noted here that Martin et al. (2008) claimed that right-bearing barbs correspond to dextral filaments and left-bearing barbs correspond to sinistral filaments. As

being hosted by a flux rope, and others by a sheared arcade. When applying this model, we have to measure the sign of helicity of the filament beforehand.

In order to calculate the sign of helicity, the vector magnetic field data SHARPs, with the 180° ambiguity resolved and projection effects corrected, are used to calculate the twist parameter $\alpha = (\nabla \times \mathbf{B})_z / B_z$, where $\mathbf{B}$ is the vector magnetic field and B_z is the line-of-sight component of $\mathbf{B}$. It was found that α in the filament channel we observed is positive, which is the preferential sign of helicity in the southern hemisphere. Since the barbs of our filament are right-bearing as indicated by Figure 4, the filament should be supported by a sheared arcade based on the indirect method proposed by Chen et al. (2014b).

Coronal magnetic extrapolation, albeit an ill-posed problem (Low 2015), provides another method to examine the host magnetic field supporting a filament. In order to perform the non-linear force-free field (NLFFF) extrapolation, we apply the optimization method (Wheatland et al. 2000; Wiegelmann 2004) with the SHARPs vector magnetogram. To remove the net force and torque on the boundary before extrapolation, data pre-processing is conducted with the method mentioned by Wiegelmann et al. (2006). The NLFFF distribution in the local Cartesian coordinates is shown in the top panels (a) and (b) of Figure 8, where magnetic field lines are superposed on the Hα-0.6 Å filtergram. The field lines are selected near the filament spine. It can be seen that the magnetic configuration near the filament spine consists of a strongly-sheared arcade as the core field (*cyan*), which is surrounded by less-sheared envelope field (*yellow*). The magnetic configuration around the south endpoint consists of some less-sheared arcades (*green*). The magnetic configuration projected onto the plane-of-the-sky is displayed in panel (b) of Figure 8.

---

pointed out by Chen et al. (2014b), this one-to-one correspondence is valid only for the inverse-polarity filaments, i.e., those supported by a magnetic flux rope. For the normal-polarity filaments, the correspondence should be exactly opposite.

It is noticed that no magnetic flux ropes are present in the extrapolated nonlinear force-free coronal field. Although the absence of magnetic dips in the extrapolated coronal field might be due to the limitation of the extrapolation method, combining the result of the repetitive moving threads near the southern endpoint of the filament, we tend to believe that the filament, at least the southern part (the green lines around the south endpoint in Hα-0.6 Å filtergram), is supported by a sheared arcade without magnetic dips.

Figure 3 reveals that the fibrils on the west side of the filament spine are left-bearing, opposite to the fibrils on the east side of the filament which are right-bearing. Comparing Figure 3 with Figure 8(b), one can see that the apparent contradiction might be simply due to the projection effects: the south leg of the yellow field lines in Figure 8(b), which are oriented toward northwest as the Hα fibrils do in Figure 3(b), are actually oriented toward northeast in the local coordinates, as illustrated by Figure 8(a). Therefore, the Hα fibrils on both sides of the filaments are actually right-bearing.

In summary, we analyzed the NST high-resolution observations of a newly formed active region filament. Based on the observations, it is shown that cool materials are injected in the form of fibrils from the chromosphere to replenish the filament suspended in the corona. Each material injection is preceded by a localized brightening in the chromosphere. It is caused by magnetic cancelation in the photosphere, implying that magnetic reconnection plays an important role in transporting chromospheric plasma into the filament. We also detected counter-streamings near the southern endpoint of the filament. We argue that the counter-streamings in this active region filament may be explained by unidirectional flows with alternative directions. This is different from many of other cases where the counter-streamings are mainly due to longitudinal oscillations of the filament threads. Nonlinear force-free field extrapolation further leads us to the conclusion that this active region filament is supported by a sheared arcade without magnetic dips. More events are

being collected from the observations of NST, New Vacuum Solar Telescope (NVST; Liu et al. 2014), and Optical and Near-infrared Solar Eruption Tracer (ONSET; Fang et al. 2013) in order to see how common these features are among active region filaments.

This work was supported by the National Natural Science Foundation of China (NSFC) under the grant numbers 11533005, 10673004, 10610099, and 11025314, as well as NKBRSF under grants 2011CB811402 and 2014CB744203. W.C. acknowledges the support of the US NSF (AGS-0847126 and AGS-1250818) and NASA (NNX13AG14G). This work was also supported by the project "The Strategic Priority Research Progran of the Chinese Academy of Sciences" (XDB09000000).

REFERENCES

Antiochos, S. K., MacNeice, P. J., Spicer, D. S. & Klimchuk, J. A. 1999, ApJ, 512, 985

Berger, T. E., Liu, W., & Low, B. C. 2012, ApJ, 758, L37

Bobra, M. G., Sun, X., Hoeksema, J. T., et al. 2014, Sol. Phys., 289, 3549

Cao, W., Gorceix, N., Coulter, R., et al. 2010, AN, 331, 636

Chae, J. 2003, ApJ, 584, 1084

Chen, P. F. 2011, LRSP, 8, 1

Chen, P. F., 2014a, in Gopalswamy, N., Hasan, S. S., Rao, P. B., & Subramanian, P. eds., ASP Conf. Ser. Vol. 10, International Symposium on Solar Terrestrial Physics, Pune, India, p. 1-10

Chen, P. F., Harra, L. K., & Fang, C. 2014b, ApJ, 784, 50

Cranmer, S. R., & Woolsey, L. N., 2015, ApJ, 812, 71

Fang, C., Chen, P. F., Li, Z. et al. 2013, RAA, 13, 1509

Gary, G. A., Hagyard, M. J. 1990, Sol. Phys., 126, 21

Gigolashvili, M. S., Japaridze, D. R., & Kukhianidze, V. J. 2013, Sol. Phys., 282, 51

Goode, P. R., & Cao, W. 2012, Proc. SPIE, 8444, 3

Guo, Y., Schmieder, B., Demoulin, P., et al., 2010, ApJ, 714, 343

Hao, Q., Fang, C., Cao, W., & Chen, P. F. 2015, ApJS, 221, 33

Hao, Q., Guo, Y., Fang, C., Chen, P. F. Cao, W. D. 2016, RAA, 16, 1

Harvey, J. W., Bolding, J., Clark, R., et al. 2011, Bulletin of the American Astronomical Society, 1745

Jiang, R. L., Shibata, K., Isobe, H., & Fang, C. 2011, ApJ, 725, L16

Karpen, J. T., Antiochos, S. K., Hohensee, M., Klimchuk, J. A., & MacNeice, P. J. 2001, ApJ, 553, L85

Karpen, J. T., Antiochos, S. K., Tanner, S. E., & DeVore, C. R. 2005, ApJ, 635, 1319

Karpen, J. T., Antiochos, S. K., & Klimchuk, J. A. 2006, ApJ, 637, 531

Karpen, J. T., & Antiochos, S. K. 2008, ApJ, 676, 658

Karpen, J. T. 2015, Plasma Structure and Dynamics In Vial J.-C., & Engvold O. eds., *Solar Prominence, ASSL*, Vol. 415, pp. 237-257, Springer

Kippenhahn, R., & Schlüter, A. 1957, ZAp, 43, 36

Kuperus, M., & Raadu, M. A. 1974, A&A, 31, 189

Lemen, J. R., Title, A. M., Akin, D. J., et al. 2012, Sol. Phys., 275, 1

Li, X., Morgan, H., Leonard, D., & Jeska, L. 2012, ApJ, 752, L22

Lin, Y., PhD Thesis, University of Oslo

Lites, B. W., & Low, B. C. 1997, Sol. Phys., 174, 91

Lites, B. W. 2005, ApJ, 622, 1275

Liu, W., Berger, T. E., & Low, B. C. 2012, ApJ, 745, L21

Liu, Z., Xu, J., Gu, B. Z. et al. 2014, RAA, 14, 705

Low B. C. 1982, Sol. Phys., 75, 119

Low, B. C. 2015, Science China Physics, Mechanics, and Astronomy, 58, 015201

Luna, M., & Karpen, J. 2012, ApJ, 750, L1

Luna, M., Moreno-Insertis, F., & Priest, E., ApJ, 808, L23

Mackay, D. H., Karpen, J. T., Ballester, J. L., Schmieder, B., & Aulanier, G. 2010, Space Sci. Rev., 151, 333

Manchester, W. B. et al. 2008, ApJ, 684, 1448

Martin, S. F., Lin, Y., & Engvold, O. 2008, Sol. Phys., 250, 31

Martin, S. F., & Ramsry, H. E. 1972, In McIntosh, P. S. ed., *Solar Activity Observations and Predictions*, p. 371

Martin, S. F., Bilimoria, R., & Tracadas, P. W. 1994, Magnetic field configurations basic to filament channels and filaments. In Rutten, R. J., & Schrijver, C. J. Eds., *Solar surface magnetism*, p. 303, Dordrecht: Kluwer Academic Publishers.

Metcalf, T. R. 1994, Sol. Phys., 155, 235

Metcalf, T. R., Leka, K. D., Barnes, G., et al. 2006, Sol. Phys., 235, 161

Minarovjech M., Rybansky M., Rusin V. 1998, Sol. Phys., 177, 357

Moore R. L., Roumeliotis G. 1992, in Svestka Z., Jackson B. V., Machado M. E., eds, IAU Colloq. 133: Eruptive Solar Flares, Vol. 399 of Lecture Notes in Physics. Springer-Verlag, Berlin, p. 69

Okamoto, T. J., Tsuneta, S., Lites, B. W., Kubo, M., Yokoyama, T., Berger, T. E. et al., 2008, ApJ, 673, L215

Ouyang, Y., Yang, K., & Chen, P. F. 2015, ApJ, 815, 72

Parenti, S. 2014, LRSP, 11, 1

Rust, D. M., & Kumar, A. 1994, Sol. Phys., 155, 69

Ryutova, M., Berger, T., Frank, Z., & Title, A. 2008, ApJ, 686, 1404

Saito, T., Kudoh, T., & Shibata, K., 2001, ApJ, 554, 1151

Scherrer, P. H., Schou, J., Bush, R. I., et al. 2012, Sol. Phys., 275, 207

Schmahl, E. J. 1982, Adv. Space Res., 2, 73

Schmieder, B., Mein, N., Deng, Y., Dumitrache, C., Malherbe, J.-M., Staiger, J. et al., 2004, Sol. Phys., 223, 119

Schmieder, B., Demoulin P., Aulanier G. 2013, Adv. Space Res., 51, 1967

Schou, J., Scherrer, P. H., Bush, R. I., et al. 2012, Sol. Phys., 275, 229

Shibata, K., & Suematsu, Y., 1982, Sol. Phys., 78, 333

Shibata, K., 1982, Sol. Phys., 81, 9

Smith E. A., Priest E. R. 1977, Sol. Phys., 53, 25

St. Cyr O. C., Webb D. F. 1991, Sol. Phys., 136, 379

Su, Y., Wang, T., Veronig, A., Temmer, M, & Gan, W., ApJ, 756, L41

Wang, Y.-M. 1999, ApJ, 520, 71

Wang, T. J., Sui, L., & Qiu, J. 2009, in Lites, B., Cheung, M., Magara, T., Mariska, J., & Reeves, K., eds, ASP Conf. Ser. Vol. 415, The Second Hinode Science Meeting, San Francisco, p. 447

Wheatland, M. S., Sturrock, P. A. & Roumeliotis, G. 2000, ApJ, 540, 1150

Wiegelmann, T. 2004, Sol. Phys., 219, 87

Wiegelmann, T., Inhester, B., & Sakurai, T. 2006, Sol. Phys., 233, 215

Xia, C., Chen, P. F., Keppens, R., & van Marle, A. J. 2011, ApJ, 737, 27

Xia, C., Chen, P. F., & Keppens, R. 2012, ApJ, 748, L26

Xia, C., Keppens, R., & Guo, Y. 2014, ApJ, 780, 130

Yelles Chaouche, L., Kuckein, C., Martinez Pillert, V., & Moreno-Insertis, F. 2012, ApJ, 748, 23

Zeldovich Y. B., & Raiser, Y. P., 1966, In Academic Press, New York and London, *Physics of Shock Waves and High Temperature Hydrodynamic Phenomena*, Vol. 1, p. 233

Zirker, J. B., Engvold, O., & Martin, S. F. 1998, Nature, 396, 440

Zhang, Q. M., Chen, P. F., Xia, C., & Keppens, R. 2012, A&A, 542, A52

Zhou, Y-H., Chen, P. F., Zhang, Q-M., & Fang, C. 2012, RAA, 14, 581

This manuscript was prepared with the AAS LaTeX macros v5.2.

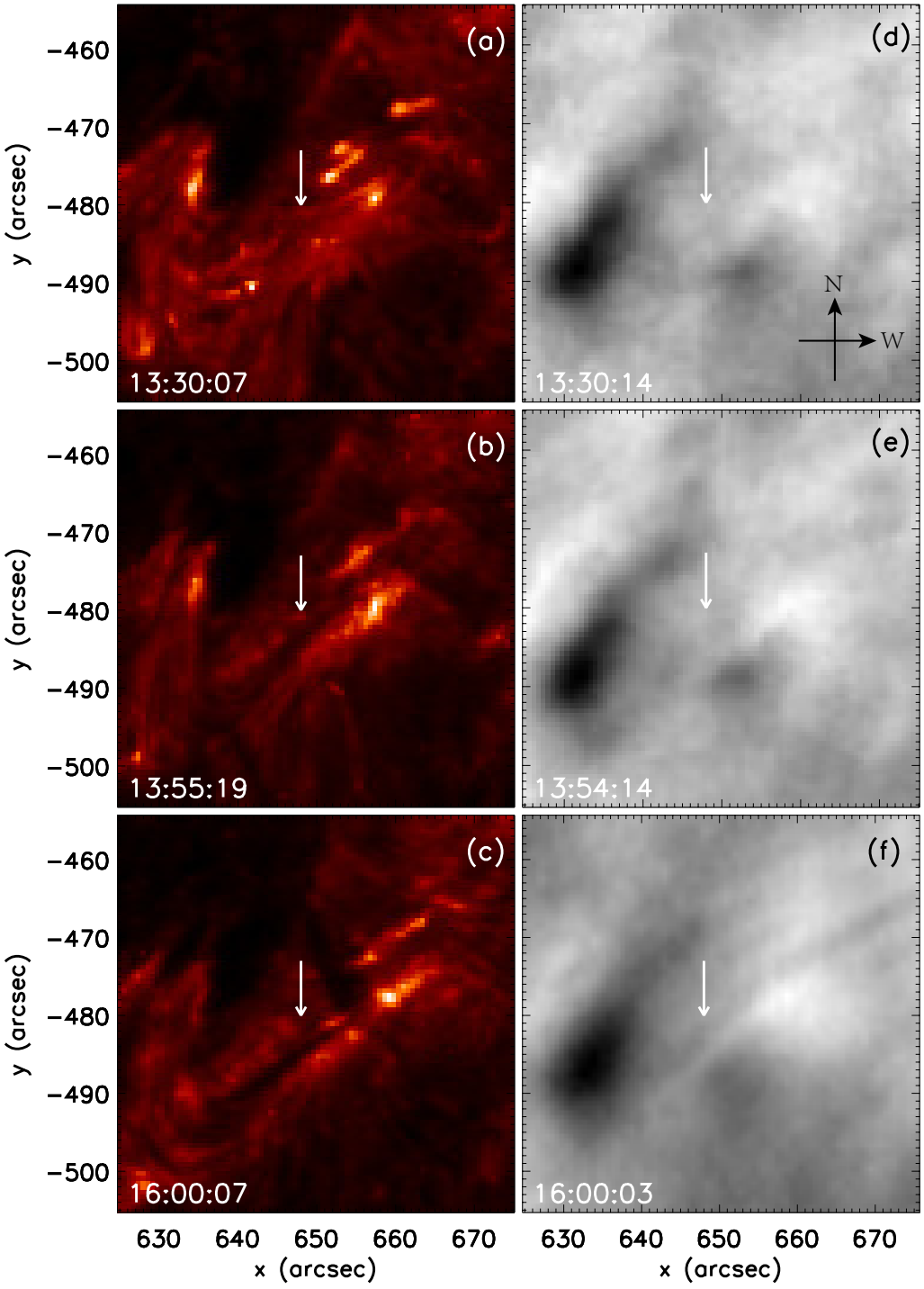

Fig. 1.— Locations and temporal evolution of the filament in 304 Å and Hα images. In panel (a) the filament is unseen in the 304 Å image. In panel (b) the filament is firstly seen and then can be clearly seen in panel (c). In panel (d) the filament is still unseen in the full-disc Hα image, and some fragments can be seen in panel (e). However, it can be obviously seen in panel (f).

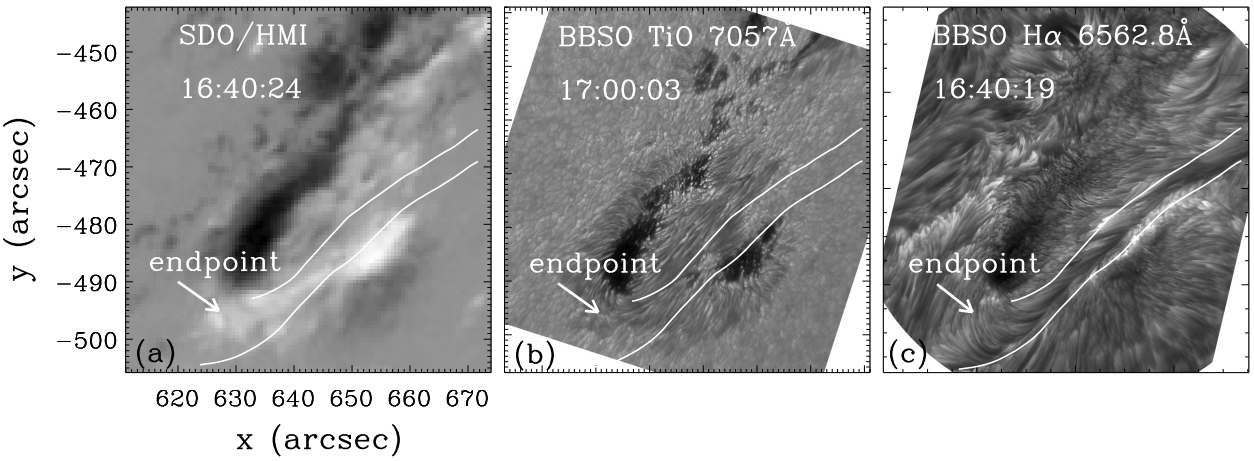

Fig. 2.— Co-aligned the images of magnetogram (a), TiO (b), and Hα line-center (c). The white lines in each panel sketch the profile of the filament. The filament endpoint is also indicated in each panel.

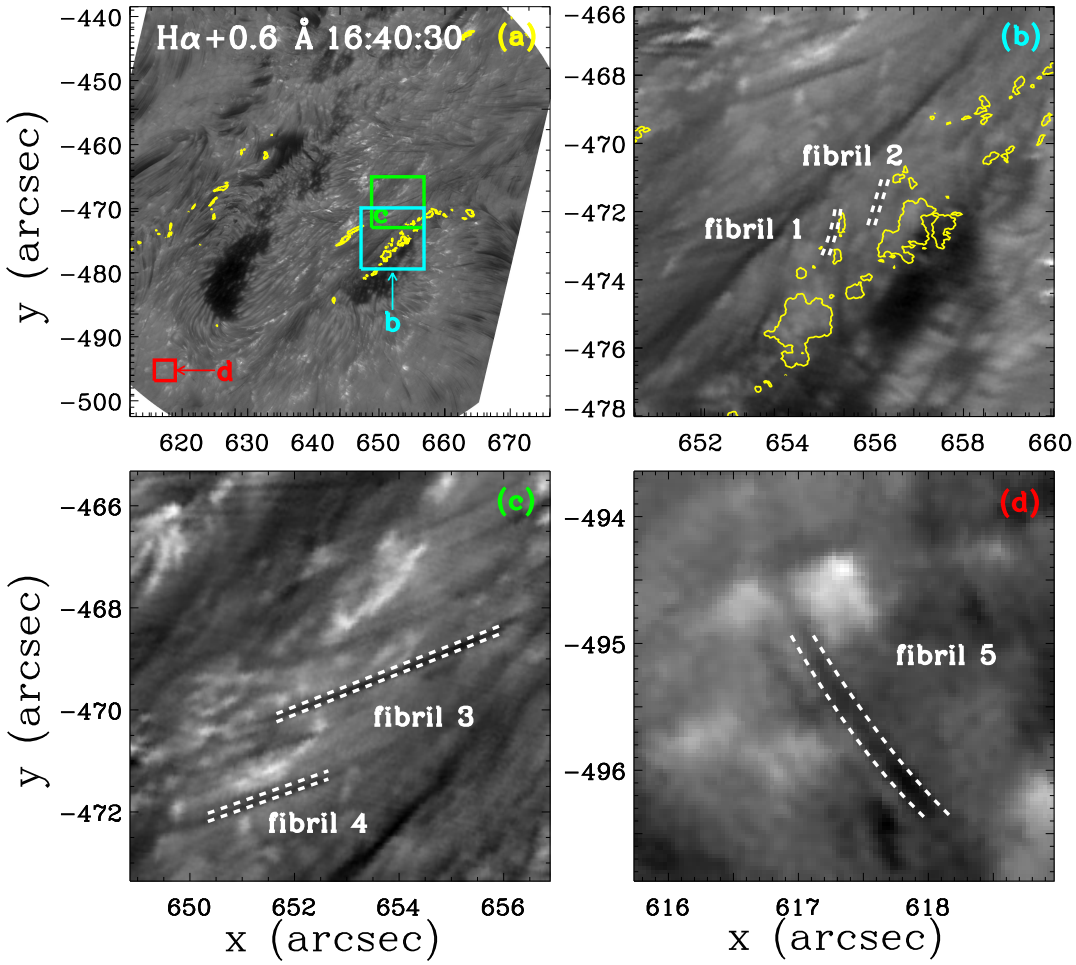

Fig. 3.— Selection of several fibrils near the filament channel. Panel (a) depicts the filament spine and the areas where we select fibrils (boxes b and c) and the endpoint of the filament (box d). Panels (b), (c), and (d) are amplified from the boxes in panel (a). The white dashed lines outline the fibrils.

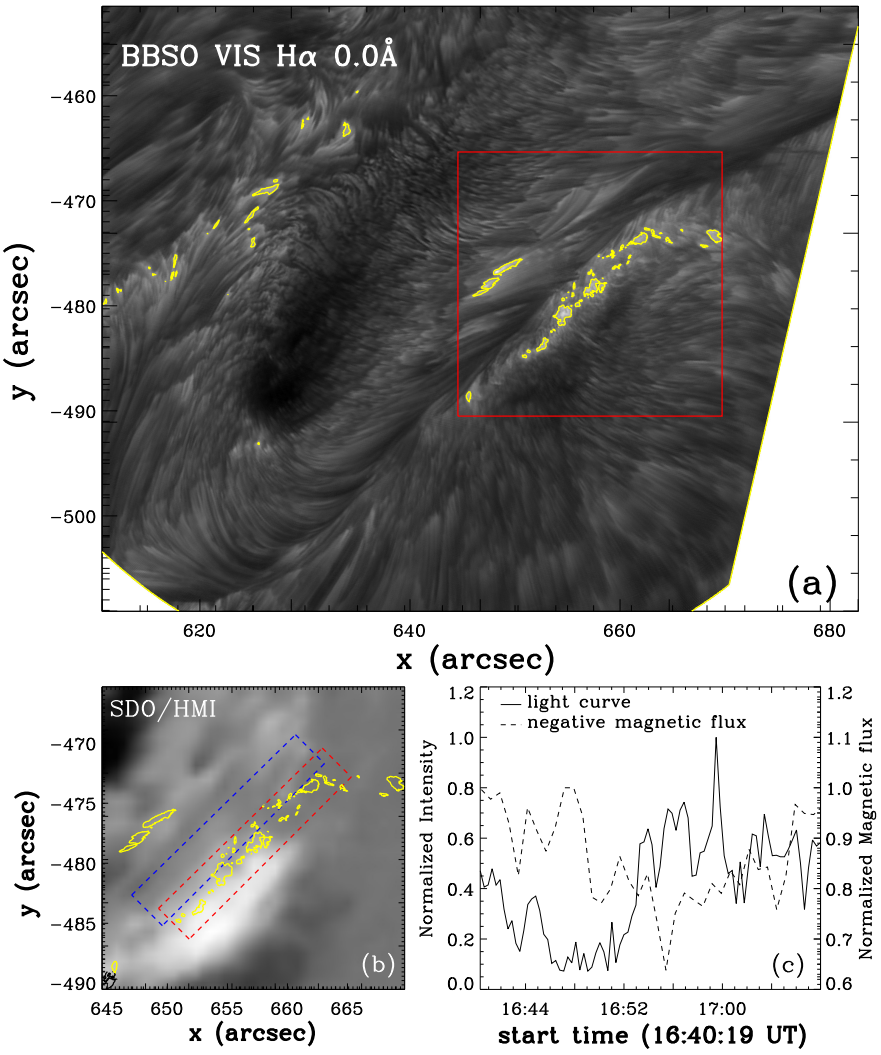

Fig. 4.— Hα line-center filtergram (a) and the associated magnetogram (b). In panel (a), bright patches are highlighted with the yellow contours, and the red box corresponds to the area of magnetogram we plot in panel (b). The red rectangular box in panel (b) shows the area we selected to calculate the lightcurve. A blue rectangular box in panel (b) shows the corresponding area in the magnetogram, with the project effect corrected. Panel (c) displays the lightcurve of the bright patches (solid line; integrated all pixels with relative intensity about twice over that of the background) and magnetic flux evolution (dashed line; integrated all the negative magnetic flux), respectively. Both curves are normalized.

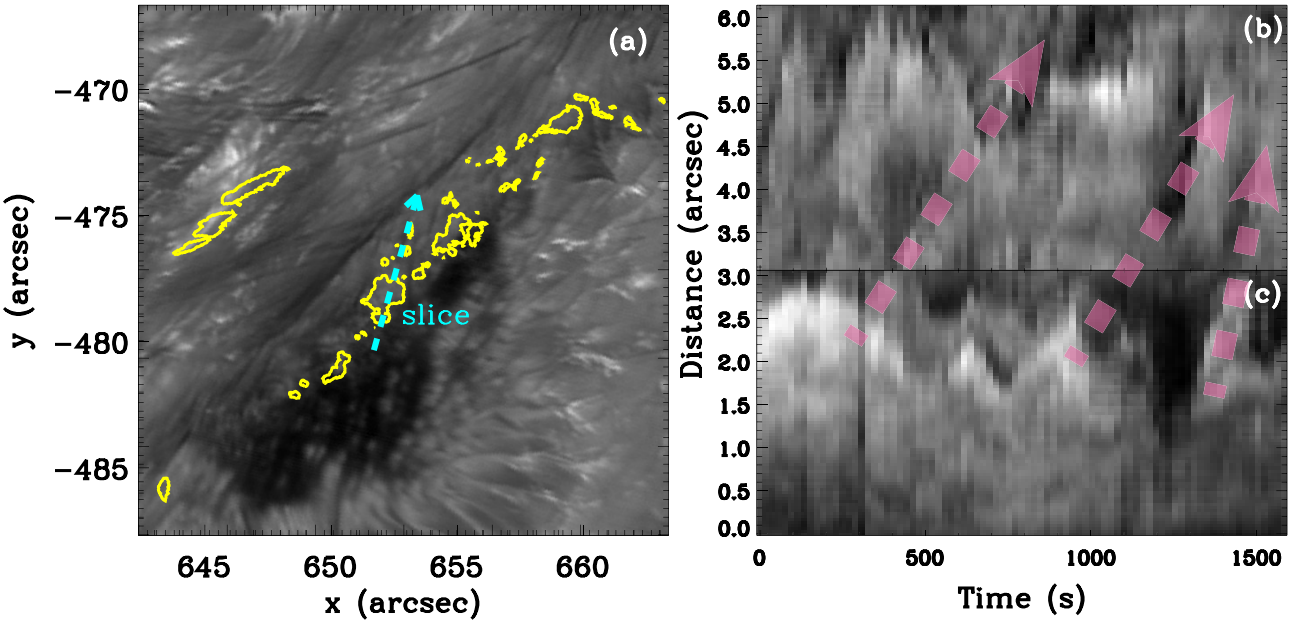

Fig. 5.— Position of the slice along the fibril 1 (panel (a); cyan dashed arrow) and its time-distance plot (panels (b) and (c)). Panel (b) is plotted by using the Hα+0.6 Å filtergram where the jet-like fibril is clearly seen. Panel (c) is plotted by using Hα center filtergram which gives the information of bright patches (yellow contour in panel (a)). Green arrows connect the bright patches and fibrils to show that an intensity enhancement in Hα center corresponds to a fibril seen in Hα red-wing filtergram.

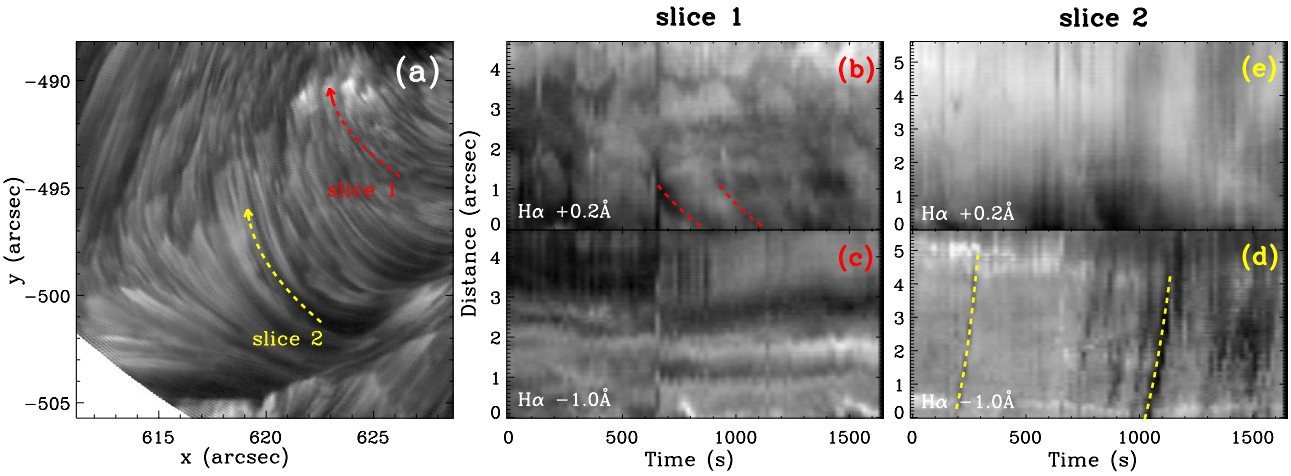

Fig. 6.— Time-distance diagrams of two fibrils near the endpoint of the filament (middle and right column). The left panel depicts the positions of two slices in different wavelengths. The middle column shows time-distance diagrams of slice 1 in red and blue wings and the right column shows the same information of slice 2. We combine these two columns to show the counter-streamings with opposite directions and they also indicate that these fibrils are unidirectional flows.

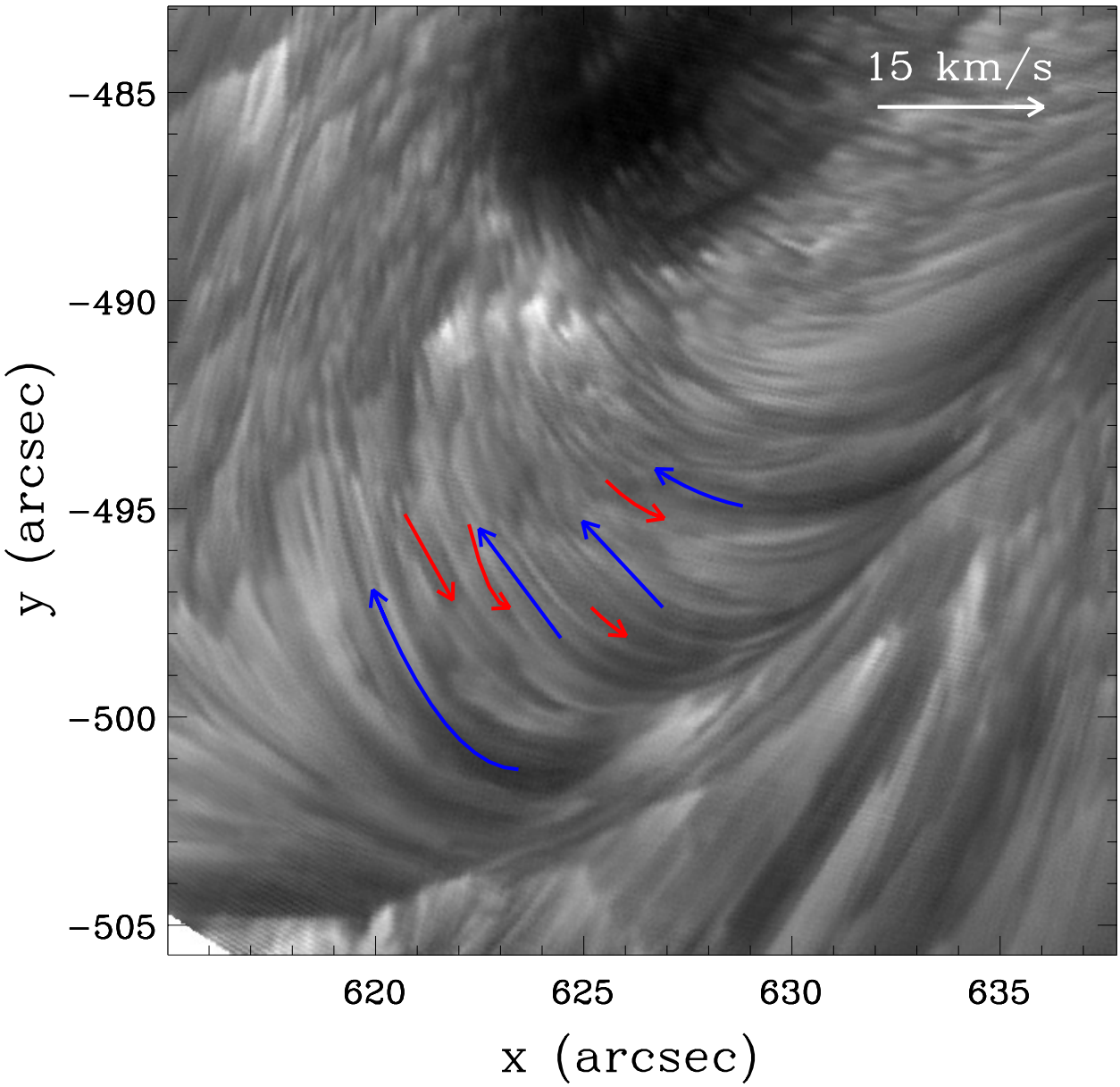

Fig. 7.— Flows near the endpoint of the filament. The red and blue arrows indicate the flow observed in Hα red-wing and blue-wing filtergrams, respectively. The length of each arrow is proportional to the local speed.

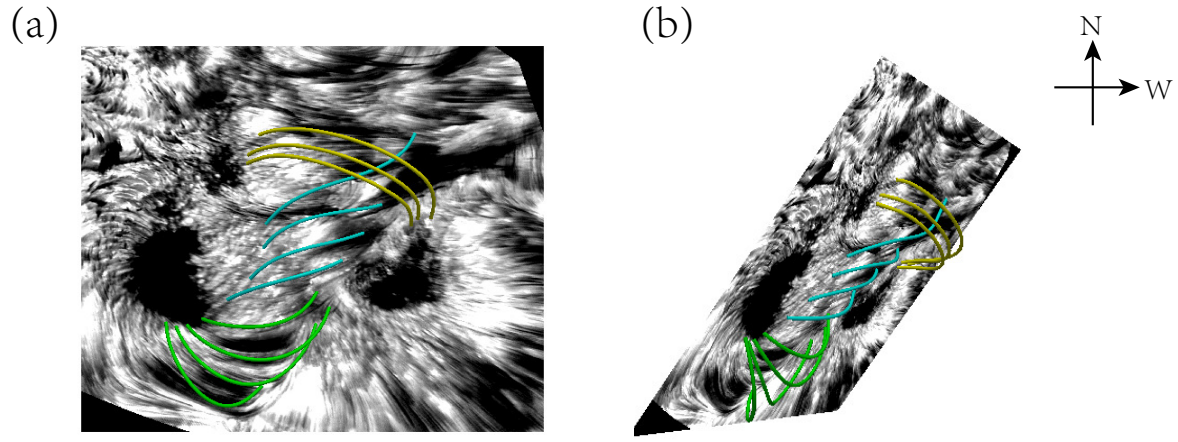

Fig. 8.— Different views of the NLFFF configuration. Panel (a) depicts the top view in the local Cartesian coordinators. Panel (b) shows the magnetic field lines projected onto the plane-of-the-sky. The backgrounds in both panels are the Hα-0.6 Å filtergram. North is upward.